Single-Layer MoS_2 Phototransistors

Zongyou Yin,[†,§] Hai Li,[†,§] Hong Li,[‡] Lin Jiang,[†] Yumeng Shi,[†] Yinghui Sun,[†] Gang Lu,[†] Qing Zhang,[‡] Xiaodong Chen,[†] and Hua Zhang[†,*]

[†]School of Materials Science and Engineering and [‡]School of Electrical and Electronic Engineering, Nanyang Technological University, 50 Nanyang Avenue, Singapore 639798. [§]These authors contributed equally to this work.

ABSTRACT

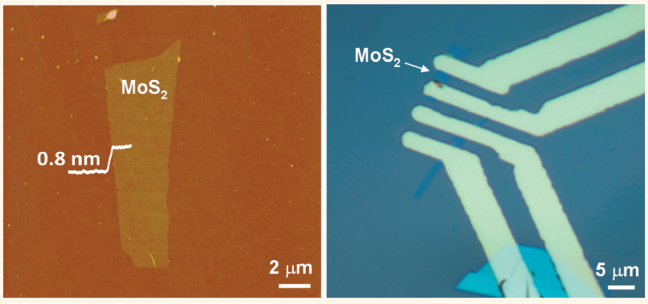

A new phototransistor based on the mechanically exfoliated single-layer MoS_2 nanosheet is fabricated, and its light-induced electric properties are investigated in detail. Photocurrent generated from the phototransistor is solely determined by the illuminated optical power at a constant drain or gate voltage. The switching behavior of photocurrent generation and annihilation can be completely finished within *ca.* 50 ms, and it shows good stability. Especially, the single-layer MoS_2 phototransistor exhibits a better photoresponsivity as compared with the graphene-based device. The unique characteristics of incident-light control, prompt photoswitching, and good photoresponsivity from the MoS_2 phototransistor pave an avenue to develop the single-layer semiconducting materials for multifunctional optoelectronic device applications in the future.

KEYWORDS: single-layer · MoS_2 · phototransistors · photocurrent · photoswitching · photoresponsivity

As one of the most promising two-dimensional (2D) materials, graphene, one-atom-thick single layer of carbon atoms packed with honeycomb lattice, has shown exceptional physical, chemical, optical and mechanical properties.[1−13] Recently, other 2D materials have attracted increasing attention.[14−22] In particular, great interest has been focusing on the single-layer semiconducting materials, such as MoS_2, one of the transition-metal dichalcogenides, which exhibits the unique physical, optical and electrical properties correlated with its 2D ultrathin atomic layer structure.[23−26] For example, the single-layer MoS_2 has a unique quantum luminescence efficiency[25,26] and exhibits a high channel mobility ($\sim 200\ cm^2V^{-1}s^{-1}$) and current ON/OFF ratio (1×10^8) when it was used as the channel material in a field-effect transistor (FET).[24]

In this contribution, to the best of our knowledge, for the first time, we fabricate the single-layer MoS_2 based phototransistor and then study its light-induced electric properties in detail. On the basis of our experimental results, we find that the photocurrent (I_{ph}) generation efficiency is dependent on the magnitude of photogenerated charges under a constant drain voltage (V_{ds}) or gate voltage (V_g). Photocurrent generation and annihilation (called as photoswitching in the text) behavior is so prompt that the photocurrent can be completely switched between ON and OFF states within *ca.* 50 ms, which is fully controlled by the incident light and exhibits a quite stable characteristic. The photoresponsivity from the single-layer MoS_2 phototransistor can reach as high as 7.5 mA/W under illumination with a low optical power (P_{light}, 80 μW) and a medium gate voltage (V_g, 50 V). Importantly, the obtained photoresponsivity from the single-layer MoS_2 is better than that obtained from the single-layer graphene based FET (1 mA/W) which mainly arises from the rapid electron−hole recombination induced by the intrinsic property of zero-bandgap and fast carrier transfer of graphene.[27,28]

RESULTS AND DISCUSSION

Preparation and Characterization of Single-Layer MoS_2-Based Phototransistors. In a typical experiment, the single-layer MoS_2 was deposited onto on a Si/SiO_2(300 nm) substrate by using the scotch-tape based mechanical exfoliation method.[29] The optical and AFM images of the obtained single-layer MoS_2 on Si/SiO_2 are shown in Figure 1A and B, respectively. The height of the single-layer MoS_2 measured by AFM is *ca.* 0.8 nm, which is consistent with the previous theoretical[30,31] and experimental[23−26,29] results. The photoluminescence (PL) of a single-layer MoS_2 sheet was measured at room temperature using

* Address correspondence to hzhang@ntu.edu.sg, hzhang166@yahoo.com.

Received for review July 3, 2011 and accepted December 13, 2011.

Published online December 13, 2011
10.1021/nn2024557

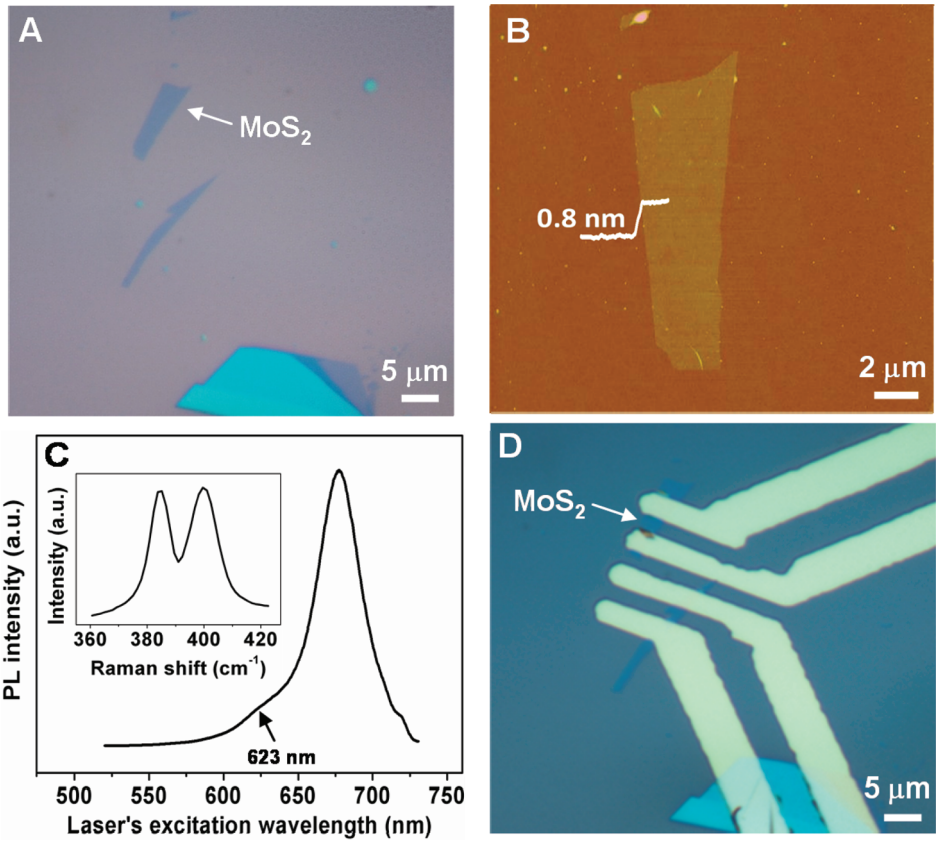

Figure 1. (A) Optical microscopy image and (B) AFM image of single-layer MoS_2. (C) PL and Raman (inset) spectra of single-layer MoS_2. (D) Optical image of FET device made by single-layer MoS_2 in (A, B).

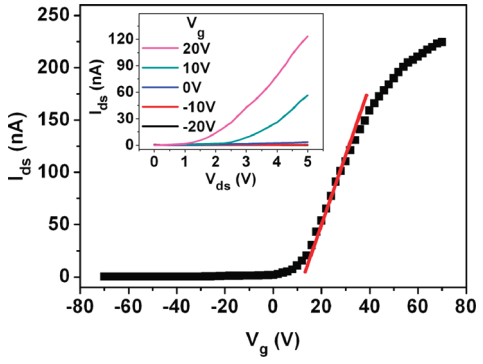

Figure 2. Room-temperature electrical characteristic of single-layer MoS_2 FET at drain voltage of 3 V. The red line is used to calculate the channel mobility. Inset: Plot of drain current (I_{ds}) *vs* voltage (V_{ds}) at different gate voltage (V_g, from −20 to 20 V).

the 488 nm laser (Figure 1C). The dominated PL peak at 676 nm arises from the direct intraband recombination of the photogenerated electron−hole pairs in the single-layer MoS_2, and the weak shoulder peak at *ca.* 623 nm is attributed to the energy split of valence band spin−orbital coupling of MoS_2.[26] Raman spectrum was used to further confirm the single-layer MoS_2 (inset in Figure 1C). Two peaks at 384 and 400 cm^{-1} are attributed to the in-plane E^1_{2g} and out-of-plane A_{1g} vibration of single-layer MoS_2, respectively.[20,29] Figure 1D shows the optical image of the single-layer MoS_2 FET device fabricated by photolithography, where two Ti/Au electrodes and Si were used as the source, drain, and back gate, respectively.

The fabricated single-layer MoS_2 FET exhibits an obvious n-type semiconducting property (Figure 2), which is consistent with the previous reports.[23,24,29] Such n-type doping might come from the impurities, such as halogen (Cl or Br) atoms, which could replace S atoms in the natural MoS_2 crystals or exist as the interstitial atoms in the interlayer gap of MoS_2. This increases the total electron concentration of the host MoS_2 system resulting in an n-type doping for MoS_2 (see more detailed discussion in the Supporting Information). The field-effect mobility of this single-layer MoS_2 device can be estimated based on the equation[24]

$$\mu = \frac{L}{W \times (\varepsilon_o \varepsilon_r / d) \times V_{ds}} \times \frac{dI_{ds}}{dV_g}$$

where the channel length L is 2.1 μm, the channel width W is 2.6 μm, ε_0 is 8.854×10^{-12} Fm^{-1}, ε_r for SiO_2 is 3.9, and d is the thickness of SiO_2 (300 nm). The calculated mobility of our device is *ca.* 0.11 $cm^2\ V^{-1}\ s^{-1}$, which is comparable with the previous results from the bottom-gate FET devices reported by other research groups.[23,24] However, the reported mobility is far lower than ~200 $cm^2\ V^{-1}\ s^{-1}$ obtained from the top-gate FET

by deposition of the high-κ gate dielectric of HfO_2, used for the device mobility booster, on the top of MoS_2.[24] The reason is likely that the trap/impurity states exist at the SiO_2 surface in the bottom gate FETs, and the scattering from these charged impurities degrades the device mobility.[24,32,33] Reduction of the surface traps/impurities in the bottom gate dielectric is expected to improve the mobility of such a single-layer MoS_2 based bottom-gate FET devices. The obtained drain current ON/OFF ratio of our device is $\sim 10^3$. Note that as compared to the mobility (*ca.* 0.03 $cm^2 V^{-1} s^{-1}$) and current ON/OFF ratio ($\sim 10^2$) from the single-layer MoS_2 FETs,[29] the enhanced mobility and ON/OFF ratio from the current single-layer MoS_2 device are attributed to the thermal annealing treatment after the device fabrication (see the Materials and Methods), which could remove the photoresist residue and improve the electrode contact.[24,34]

Photocurrent Dependence on the Incident Optical Power. The single-layer MoS_2 based phototransistor was investigated by exploring its output characteristics of photocurrent, including the generation, switching behavior and photoresponsivity, in various optical power and applied gate voltage. As shown in Figure 3A, when the excitation wavelength was above $\sim$670 nm, the generated photocurrent, obtained after reduction of the dark drain current, was quite low. However when the wavelength decreased from 670 nm, the generated photocurrent increased obviously. This is reasonable since the photocurrent generation needs to match the basic condition, that is, the incident photon energy must be greater than the energy gap (E_g) of single-layer MoS_2, which is around 1.83 eV, that is, 676 nm in wavelength.[26] Only those incident photons with large energy ($h\nu > 1.83$ eV, that is, wavelength < 676 nm) can excite electrons from the valence band (VB) to the conduction band (CB) in the single-layer MoS_2, generating the photocurrent when the drain voltage is applied. On the other hand, when the incident photon energy is above the E_g of MoS_2, the photocurrent is mainly dependent on the incident optical power and the transition probability of photoexcited electrons (or photoelectrons). Photons with higher energy, that is, shorter wavelength, will transfer more energy to electrons which have a higher probability to overcome the defect/impurity trapping of MoS_2, further overpass the Au:Ti/MoS_2 Schottky barrier, and then flow to the external circuit to generate the photocurrent. In other words, the transition probability of photoelectrons, contributing to the photocurrent, is higher under the illumination of higher-energy photons. These high-energy photons can generate larger photocurrent as observed in Figure 3A. However, an increase of the photon energy leads to the decrease of its number under a constant optical power, which compromises the photocurrent increase. Therefore, the net increase rate of photocurrent becomes slow as the photon energy increases (Figure 3A).

Under the constant excitation wavelength at 550 nm, even the optical power is less than 100 μW, the illumination on the single-layer MoS_2 can generate an obvious photocurrent which is power dependent. As shown in Figure 3B, when the optical power increases from 10 to 80 μW, the photocurrent increases gradually, even the applied drain voltage is less than 1 V. To study the relationship between the output photocurrent (I_{ph}) and the incident optical power (P_{light}), the plot of I_{ph} as function of P_{light} is shown in Figure 3C, based on the results in Figure 3B. The I_{ph} under the constant drain voltage is linearly proportional to P_{light}. Such a relation has been described by the equation,[35] $I_{ph} = (q\mu_p pE)WD = CP_{light}$, where q is the electronic charge, μ_p is the charge carrier mobility, p is the charge carrier concentration, E is the electrical field in the channel, W is the gate width, D is the depth of the absorption region, C is the fitting parameter, and P_{light} is the incident optical power. In such a single-layer MoS_2 based phototransistor, the linear relation of I_{ph} *vs* P_{light} confirms that the photocurrent is solely determined by the amount of photogenerated carriers under illumination.

Prompt Photoswitching and Good Stability. The photoswitching characteristic and stability of single-layer MoS_2 phototransistors were investigated at room temperature in air. As shown in Figure 4A, the photocurrent as a function of time was measured under the alternative dark and illumination conditions at different optical power and drain voltage. The switching behavior of drain current, that is, the current ramps to a high value (ON state) under illumination and resumes to the low value (OFF state) under dark, was clearly observed. The generated photocurrent increases with the incident optical power and drain voltage. For example, when the optical power changes from 30 to 80 μW at constant drain voltage of 1 V, as expected, the photocurrent increases from 1.0 to 3.1 nA. Note that the photocurrent further increases from 3.1 to 77.5 nA when the drain voltage increases from 1 to 7 V at constant optical power of 80 μW (Figure 4A). Such drain-voltage-dependent photocurrent generation indicates that some photogenerated charge carriers cannot be converted to the photocurrent when the applied drain voltage is low. This is reasonable since a larger drain voltage can better drive photogenerated charges to electrode, or suppress photogenerated charges from the recombination.

To study the photoswitching behavior of a single-layer MoS_2 phototransistor, the change of photocurrent was recorded in a short time scale (Figure 4B). The observed switching duration for the current rise (from OFF to ON) or decay (from ON to OFF) process is only *ca.* 50 ms. In particular, such prompt photoswitching behavior can be obtained at different V_{ds} or P_{light}.

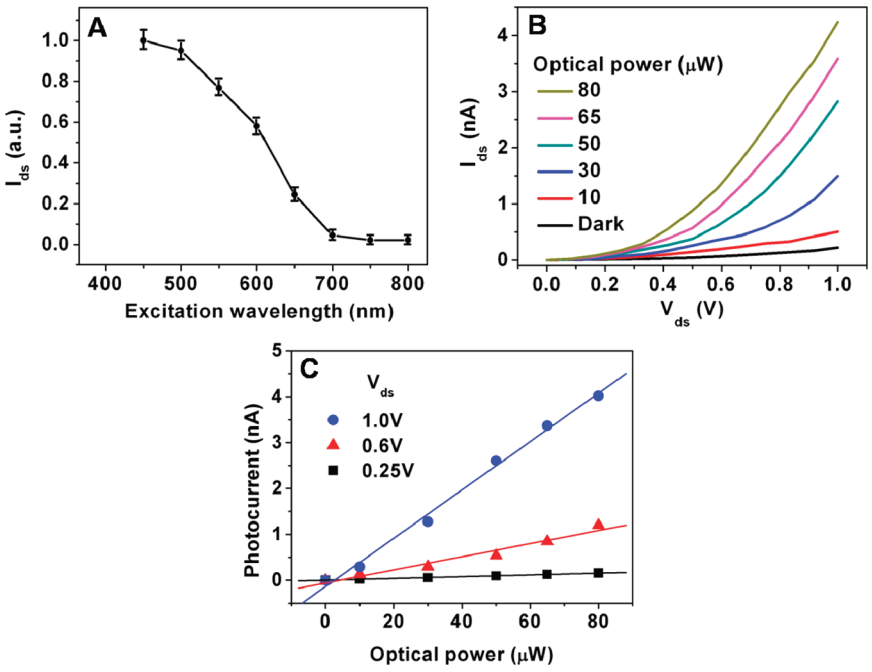

Figure 3. (A) Drain current (I_{ds}) as a function of excitation wavelength of the illumination source at a constant optical power of 80 μW. The I_{ds} values were obtained by measuring three single-layer MoS_2 phototransistors. (B) Typical output characteristics of phototransistor at different illuminating optical power (10 to 80 μW) at $V_g = 0$ V. (C) Dependence of photocurrent on optical power at different V_{ds} (0.25, 0.6, and 1.0 V). The linear curves are fitting results.

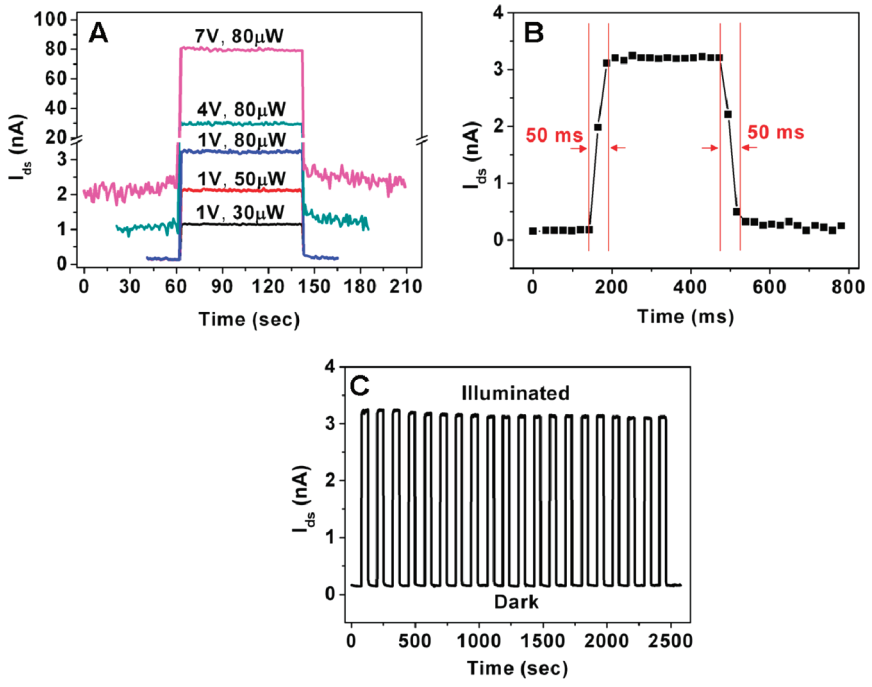

Figure 4. (A) Photoswitching characteristics of single-layer MoS_2 phototransistor at different optical power (P_{light}) and drain voltage (V_{ds}). (B) Photoswitching rate and (C) stability test of photoswitching behavior of single-layer MoS_2 phototransistor at $V_{ds} = 1$ V, $P_{light} = 80$ μW.

Moreover, the stability of this switching behavior was demonstrated by applying multiple illumination on the device for ~50 s. As shown in Figure 4C, the ON−OFF switching behavior can be well retained even after 20-cycle repeats. However, the response rate of photocurrent in our single-layer MoS_2 is still lower than that from graphene (tens of picoseconds), as the carrier transport in graphene is ballistic and very fast.[27,28]

Good Photoresponsivity Tailored by Gate Voltage. The photocurrent generation efficiency can be further enhanced by introduction of the gate voltage. In a typical experiment, if the gate voltage varies from −30 to 50 V,

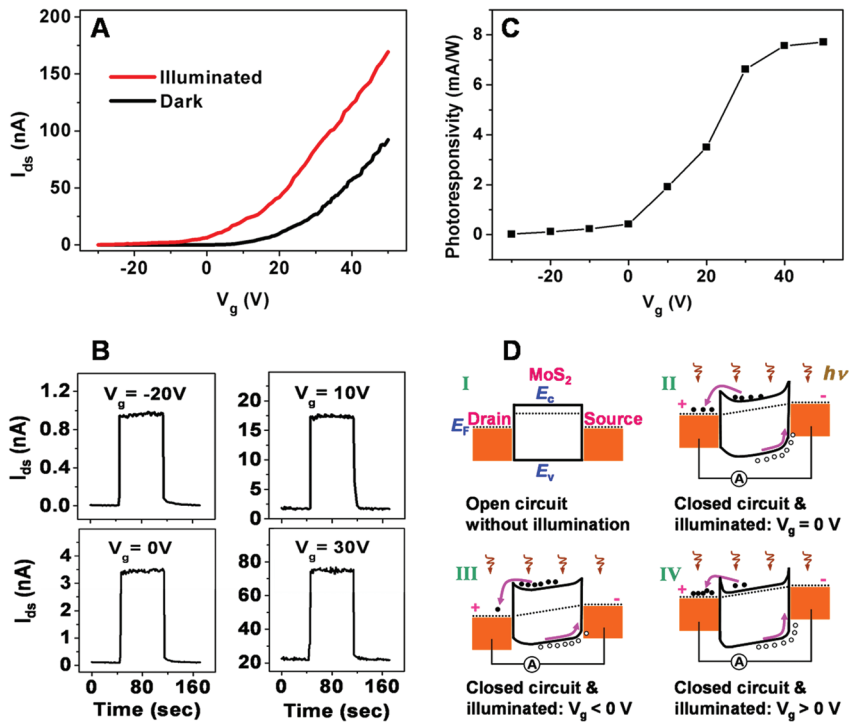

Figure 5. (A) Typical output characteristics of single-layer MoS_2 phototransistor at gate voltage varied from −30 to 50 V (P_{light} = 80 μW). (B) Similar prompt photoswitching behavior at different gate voltage (V_{ds} = 1 V, P_{light} = 80 μW). (C) Dependence of photoresponsivity on the gate voltage (V_{ds} = 1 V, P_{light} = 80 μW). (D) Diagram of single-layer MoS_2 phototransistor circuit: Diagram I represents the initial state of device under open circuit without illumination. Diagrams II, III, and IV represent the device under short circuit (source-drain voltage V_{ds} = 1 V) and illumination (P_{light} = 80 μW) while different gate voltages (V_g) were applied. The full dots at conduction band energy level (E_c) and the empty dots at valence band energy level (E_v) in MoS_2 represent the photoexcited electrons and holes, respectively. The conduction band energy level of MoS_2 is set at ~4.5 eV.[38] The valence band energy level of single-layer MoS_2 is ~6.3 eV because of its energy gap of ~1.8 eV. The Fermi level of MoS_2 is set at 4.7 eV. The Fermi level of Au is 5.1 eV.

while P_{light} and V_{ds} are kept at 80 μW and 1 V, respectively, the recorded drain current under illumination is higher than that under dark (Figure 5A). Moreover, the prompt photocurrent ON/OFF switching behavior is still well maintained in the range of applied gate voltage, which could be seen from the similar prompt photocurrent switching results under the different gate voltage as shown in Figure 5B. All these results further confirm the good stability of our single-layer MoS_2 phototransistor and also demonstrate that the photocurrent can be tailored with the incident optical power, drain, or gain voltage.

Photoresponsivity, a critical parameter to evaluate the performance of a phototransistor, is defined as photoresponsivity = I_{ph}/P_{light}, where I_{ph} is the generated photocurrent and P_{light} is the total incident optical power on the MoS_2.[27] On the basis of the photocurrent generated under different gate voltage, the calculated photoresponsivity as function of the gate voltage is plotted in Figure 5C. Under the zero gate voltage, the photoresponsivity is ~0.42 mA/W with P_{light} and V_{ds} set at 80 μW and 1 V, respectively. However, it reaches as high as 7.5 mA/W at the gate voltage of ~50 V, proving that the back gate plays an important role in tailoring the photocurrent in the n-type single-layer MoS_2 phototransistor. Admittedly, the photoresponsivity from our single layer MoS_2 phototransistor is low as compared to the reported phototransistors based on ZnO nanowires (1.29×10^4 A/W) or vertical Si nanowire arrays (~ 10^5 A/W),[36,37] but it is higher than that in the 2D graphene based devices, ~1 mA/W at a gate voltage of 60 V.[27,28] The lower photoresponsivity from graphene, as compared with our single-layer MoS_2, is probably due to the intrinsic zero bandgap, fast carrier transport and a short photocarrier lifetime in graphene which may trigger a fast recombination of the photogenerated carriers. The higher photoresponsivity from the one-dimensional ZnO or Si nanowire-based phototransistors, as compared to single layer MoS_2 or graphene-based devices, might be due to the material dimensions or other factors, which needs further study.

The gate voltage dependent photoresponsivity in our single-layer MoS_2 photransistor is attributed to the n-type doping of MoS_2. As schematically illustrated in Figure 5D, before contact, Au and MoS_2 have a different Fermi level (E_F, Figure 5D-I). The equilibrium state will be reached upon the contact between Au and MoS_2, thus forming a new quasi-Fermi level (E_{QF}, Figure 5D−II). Note that, here, the gate voltage has not been applied and the Ti bonding layer is not considered in terms of Fermi level since its thickness is only *ca.* 3 nm, much thinner than the Au electrode layer (50 nm). However, if

the negative gate voltage is applied, E_{QF} moves from CB to VB of MoS_2, resulting in a larger barrier between the CB of MoS_2 and the E_{QF} of Au electrode (Figure 5D-III) as compared to the state at zero gate voltage (Figure 5D-II). Therefore, the photogenerated charges difficultly drift to the external circuit, resulting in a low photocurrent generated. On the contrary, if the applied gate is positive, E_{QF} approaches closer to the CB of MoS_2, forming a smaller barrier between the CB of MoS_2 and the E_{QF} of the Au electrode (Figure 5D-IV) as compared with the state under zero gate voltage (Figure 5D-II), leading to the photogenerated charges which drift efficiently to the external circuit to produce a high photocurrent.

CONCLUSIONS

In summary, for the first time, we fabricate the mechanically exfoliated single-layer MoS_2 based phototransistor and investigate its electric characteristics in detail. The photocurrent generation solely depends on the illuminating optical power at a constant drain or gate voltage. Photocurrent generation and annihilation can be switched within *ca.* 50 ms. Such prompt photoswitching behavior, controllable by the incident light, exhibits stable characteristics. Importantly, the single-layer MoS_2 phototransistor gives a better photoresponsivity than does the graphene-based device. Overall, the unique characteristics, such as incident-light control, prompt photoswitching, and good photoresponsivity, of the single-layer MoS_2 phototransistor encourage one to fabricate the optoelectronic device based on single atomic layer semiconductors by a facile and low-cost mechanic exfoliation method. This work opens an avenue to develop single-layer semiconducting materials for future functional device applications in switches, memories, signal-amplifiers, and light-related sensors, *etc*.

MATERIALS AND METHODS

Deposition of MoS_2 on Si/SiO_2 Substrate. A single-layer MoS_2 sheet was peeled from a bulk MoS_2 sample (429MM-AB, SPI molybdenum disulfide, natural single crystals from Canada, CAS No.: 1317-33-5, RTECS No.: QA4697000) and deposited onto a cleaned Si/SiO_2(300 nm) substrate using cellophane tape-based exfoliation.[29] An optical microscope (Eclipse LV100, Nikon) was used to locate the target MoS_2 sheets. AFM (Dimension 3100 with Nanoscope IIIa controller, Veeco), working under the tapping mode in air, was used to measure the thickness of the MoS_2 sheets in order to confirm their layer numbers.

Photoluminescence and Raman Spectroscopy. The single-layer MoS_2 were characterized by photoluminescence (PL) and Raman spectroscopy at room temperature (both measured on a WITec CRM200 confocal Raman microscopy system) at the excitation line of 488 nm and an air cooling charge coupled device (CCD) as the detector (WITec Instruments Corp, Germany). The Raman band of Si at 520 cm^{-1} was used as a reference to calibrate the spectrometer.

Fabrication and Characterization of Single-Layer MoS_2 Phototransistors. The phototransistor has the similar configuration of the field-effect transistor (FET) while the incident illumination light source was used to tailor the photocurrent. The light source was set up based on the monochromator which has an adjustable wavelength of 400−1000 nm and optical power of 10−80 μW. The spot size of the incident light is $\sim 10 \times 10\ \mu m^2$, which covers the full MoS_2 channel and two Ti/Au electrodes. Note that the dominant photocurrent in the circuit is from MoS_2 since the same work function material Ti/Au is used as the source and drain electrodes. The electrode patterns for the source and drain of device were defined by the conventional photolithography and the lift-off process. The 3-nm-Ti/50-nm-Au source and drain electrodes were deposited by electron beam evaporation. After removing the photoresist by acetone, the fabricated phototransistor were annealed for 2 h in a vacuum tube furnace with 100 sccm $Ar:H_2$ (v/v = 9:1) flow at 200 °C to remove the photoresist residue and improve the contact for devices.[24,34] Finally, the electrical properties of the single-layer MoS_2 phototransistor were tested at room temperature in air.

Acknowledgment. This work was supported by AcRF Tier 2 (ARC 10/10, No. MOE2010-T2-1-060) from MOE, Singapore National Research Foundation under CREATE programme: Nanomaterials for Energy and Water Management, and New Initiative Fund FY 2010 (M58120031) from NTU in Singapore.

Supporting Information Available: Additional figures as described in the text. This material is available free of charge *via* the Internet at http://pubs.acs.org.

REFERENCES AND NOTES

1. Geim, A. K.; Novoselov, K. S. The Rise of Graphene. *Nat. Mater.* **2007**, *6*, 183–191.
2. Huang, X.; Qi, X. Y.; Boey, F.; Zhang, H. Graphene-Based Composites. *Chem. Soc. Rev.* **2012**, DOI: 10.1039/C1CS15078B.
3. Huang, X.; Yin, Z. Y.; Wu, S. X.; Qi, X. Y.; He, Q. Y.; Zhang, Q. C.; Yan, Q. Y.; Boey, F.; Zhang, H. Graphene-Based Materials: Synthesis, Characterization, Properties and Applications. *Small* **2011**, *7*, 1876–1902.
4. Stoller, M. D.; Park, S.; Zhu, Y.; An, J.; Ruoff, R. S. Graphene-Based Ultracapacitors. *Nano Lett.* **2008**, *8*, 3498–3502.
5. Jiang, H. J. Chemical Preparation of Graphene-Based Nanomaterials and Their Applications in Chemical and Biological Sensors. *Small* **2011**, *7*, 2413–2427.
6. Yin, Z. Y.; Sun, S.; Salim, T.; Wu, S. X.; Huang, X.; He, Q. Y.; Lam, Y. M.; Zhang, H. Organic Photovoltaic Devices Using Highly Flexible Reduced Graphene Oxide Films as Transparent Electrodes. *ACS Nano* **2010**, *4*, 5263–5268.
7. Yin, Z. Y.; Wu, S. X.; Zhou, X. Z.; Huang, X.; Zhang, Q. C.; Boey, F.; Zhang, H. Electrochemical Deposition of ZnO Nanorods on Transparent Reduced Graphene Oxide Electrodes for Hybrid Solar Cells. *Small* **2010**, *6*, 307–312.
8. Huang, X.; Li, S. Z.; Huang, Y. Z.; Wu, S. X.; Zhou, X. Z.; Li, S. Z.; Gan, C. L.; Boey, F.; Mirkin, C. A.; Zhang, H. Synthesis of Hexagonal Close-Packed Gold Nanostructures. *Nat. Commun.* **2011**, *2*, 292.
9. Qi, X. Y.; Pu, K. Y.; Li, H.; Zhou, X. Z.; Wu, S. X.; Fan, Q. L.; Liu, B.; Boey, F.; Huang, W.; Zhang, H. Amphiphilic Graphene Composites. *Angew. Chem., Int. Ed.* **2010**, *49*, 9426–9429.
10. He, Q. Y.; Sudibya, H. G.; Yin, Z. Y.; Wu, S. X.; Li, H.; Boey, F.; Huang, W.; Chen, P.; Zhang, H. Centimeter-Long and Large-Scale Micropatterns of Reduced Graphene Oxide Films: Fabrication and Sensing Applications. *ACS Nano* **2010**, *4*, 3201–3208.
11. Huang, X.; Zhou, X. Z.; Wu, S. X.; Wei, Y. Y.; Qi, X. Y.; Zhang, J.; Boey, F.; Zhang, H. Reduced Graphene Oxide-Templated Photochemical Synthesis and *in situ* Assembly of Au Nanodots to Orderly Patterned Au Nanodot Chains. *Small* **2010**, *6*, 513–516.
12. Qi, X. Y.; Pu, K. Y.; Zhou, X. Z.; Li, H.; Liu, B.; Boey, F.; Huang, W.; Zhang, H. Conjugated-Polyelectrolyte-Functionalized

Reduced Graphene Oxide with Excellent Solubility and Stability in Polar Solvents. *Small* **2010**, *6*, 663–669.
13. Song, J. L.; Yin, Z. Y.; Yang, Z. J.; Amaladass, P.; Wu, S. X.; Ye, J.; Zhao, Y.; Deng, W. Q.; Zhang, H.; Liu, X. W. Enhancement of Photogenerated-Electron Transport in Dye-Sensitized Solar Cells with Introduction of Reduced Graphene Oxide–TiO_2 Junction. *Chem.—Eur. J.* **2011**, *17*, 10832–10837.
14. Coleman, J. N.; Lotya, M.; O'Neill, A.; Bergin, S. D.; King, P. J.; Khan, U.; Young, K.; Gaucher, A.; De, S.; Smith, R. J.; *et al*. Two-Dimensional Nanosheets Produced by Liquid Exfoliation of Layered Materials. *Science* **2011**, *331*, 568–571.
15. Shi, Y.; Hamsen, C.; Jia, X.; Kim, K. K.; Reina, A.; Hofmann, M.; Hsu, A. L.; Zhang, K.; Li, H.; Juang, Z.; *et al*. Synthesis of Few-Layer Hexagonal Boron Nitride Thin Film by Chemical Vapor Deposition. *Nano Lett.* **2010**, *10*, 4134–4139.
16. Du, G.; Guo, Z.; Wang, S.; Zeng, R.; Chen, Z.; Liu, H. Superior Stability and High Capacity of Restacked Molybdenum Disulfide as Anode Material for Lithium Ion Batteries. *Chem. Commun.* **2010**, *46*, 1106–1108.
17. Chang, K.; Chen, W. *In situ* Synthesis of MoS_2/Graphene Nanosheet Composites with Extraordinarily High Electrochemical Performance for Lithium Ion Batteries. *Chem. Commun.* **2011**, *47*, 4252–4254.
18. Okamoto, H.; Kumai, Y.; Sugiyama, Y.; Mitsuoka, T.; Nakanishi, K.; Ohta, T.; Nozaki, H.; Yamaguchi, S.; Shirai, S.; Nakano, H. Silicon Nanosheets and Their Self-Assembled Regular Stacking Structure. *J. Am. Chem. Soc.* **2010**, *132*, 2710–2718.
19. Yu, T.; Lim, B.; Xia, Y. Aqueous-Phase Synthesis of Single-Crystal Ceria Nanosheets. *Angew. Chem., Int. Ed.* **2010**, *49*, 4484–4487.
20. Lee, C.; Yan, H.; Brus, L. E.; Heinz, T. F.; Hone, J.; Ryu, S. Anomalous Lattice Vibrations of Single- and Few-Layer MoS_2. *ACS Nano* **2010**, *4*, 2695–2700.
21. Osada, M.; Sasaki, T. Exfoliated Oxide Nanosheets: New Solution to Nanoelectronics. *J. Mater. Chem.* **2009**, *19*, 2503–2511.
22. Gorbachev, R. V.; Riaz, I.; Nair, R. R.; Jalil, R.; Britnell, L.; Belle, B. D.; Hill, E. W.; Novoselov, K. S.; Watanabe, K.; Taniguchi, T.; *et al*. Hunting for Monolayer Boron Nitride: Optical and Raman Signatures. *Small* **2011**, *7*, 465–468.
23. Novoselov, K. S.; Jiang, D.; Schedin, F.; Booth, T. J; Khotkevich, V. V.; Morozov, S. V.; Geim, A. K. Two-Dimensional Atomic Crystals. *Proc. Natl. Acad. Sci. U.S.A.* **2005**, *102*, 10451–10453.
24. Radisavljevic, B.; Radenovic, A.; Brivio, J.; Giacometti, V.; Kis, A. Single-Layer MoS_2 Transistors. *Nat. Nanotechnol.* **2011**, *6*, 147–150.
25. Mak, K. F.; Lee, C.; Hone, J.; Shan, J.; Heinz, T. F. Atomically Thin MoS_2: A New Direct-Gap Semiconductor. *Phys. Rev. Lett.* **2010**, *105*, 136805.
26. Splendiani, A.; Sun, L.; Zhang, Y. B.; Li, T. S; Kim, J.; Chim, C. Y.; Galli, G.; Wang, F. Emerging Photoluminescence in Monolayer MoS_2. *Nano Lett.* **2010**, *10*, 1271–1275.
27. Xia, F.; Mueller, T.; Lin, Y.; Valdes-Garcia, A.; Avouris, P. Ultrafast Graphene Photodetector. *Nat. Nanotechnol.* **2009**, *4*, 839–843.
28. Xia, F.; Mueller, T.; Golizadeh-Mojarad, R.; Freitag, M.; Lin, Y.; Tsang, J.; Perebeinos, V.; Avouris, P. Photocurrent Imaging and Efficient Photon Detection in a Graphene Transistor. *Nano Lett.* **2009**, *9*, 1039–1044.
29. Li, H.; Yin, Z. Y.; He, Q. Y.; Li, H.; Huang, X.; Lu, G.; Fam, D. W. H.; Tok, A. I. Y.; Zhang, Q.; Zhang, H. Fabrication of Single- and Multilayer MoS_2 Film-Based Field Effect Transistors for Sensing NO at Room Temperature. *Small* **2012**, DOI: 10.1002/smll.201101016.
30. Wilson, J. A.; Yoffe, A. D. The Transition Metal Dichalcogenides Discussion and Interpretation of the Observed Optical, Electrical and Structural Properties. *Adv. Phys.* **1969**, *18*, 193–335.
31. Mattheis, L. F. Band Structures of Transition-Metal-Dichalcogenide Layer Compounds. *Phys. Rev. B* **1973**, *8*, 3719–3740.
32. Chen, J. H.; Jang, C.; Adam, S.; Fuhrer, M. S.; Williams, E. D.; Ishigami, M. Charged-Impurity Scattering in Graphene. *Nat. Phys.* **2008**, *4*, 377–381.
33. Ghatak, S.; Pal, A. N.; Ghosh, A. Nature of Electronic States in Atomically Thin MoS_2 Field-Effect Transistors. *ACS Nano* **2011**, *5*, 7707–7712.
34. Ishigami, M.; Chen, J. H.; Cullen, W. G.; Fuhrer, M. S.; Williams, E. D. Atomic Structure of Graphene on SiO_2. *Nano Lett.* **2007**, *7*, 1643–1648.
35. Sze, S. M.; Ng, K. K. *Physics of Semiconductor Devices*, 3rd ed.; Wiley: New York, 2007.
36. Weng, W. Y.; Chang, S. J.; Hsu, C. L.; Hsueh, T. J. A ZnO-Nanowire Phototransistor Prepared on Glass Substrates. *ACS Appl. Mater. Interfaces* **2011**, *3*, 162–166.
37. Zhang, A.; Kim, H.; Cheng, J.; Lo, Y. H. Ultrahigh Responsivity Visible and Infrared Detection Using Silicon Nanowire Phototransistors. *Nano Lett.* **2010**, *10*, 2117–2120.
38. Abrams, B. L.; Wilcoxon, J. P. Nanosize Semiconductors for Photooxidation. *Crit. Rev. Solid State Mater. Sci.* **2005**, *30*, 153–182.